JOURNAL OF GEOPHYSICAL RESEARCH, VOL. 97, NO. D5, PAGES 5885–5893, APRIL 20, 1992

Arctic Ice Surface Temperature Retrieval from AVHRR Thermal Channels

J. KEY and M. HAEFLIGER

Cooperative Institute for Research in Environmental Sciences, University of Colorado, Boulder

The relationship between AVHRR thermal radiances and the surface (skin) temperature of Arctic snow-covered sea ice is examined through forward calculations of the radiative transfer equation, providing an ice/snow surface temperature retrieval algorithm for the central Arctic Basin. Temperature and humidity profiles with cloud observations collected on an ice island during 1986-1987 are used. Coefficients that correct for atmospheric attenuation are given for three Arctic clear sky "seasons", as defined through statistical analysis of the daily profiles, for the NOAA 7, 9, and 11 satellites. Modeled directional snow emissivities, different in the two split-window (11 and 12 μm) channels, are used. While the sensor scan angle is included explicitly in the correction equation, its effect in the dry Arctic atmosphere is small, generally less than 0.1 K. Using the split-window channels and scan angle, the rms error in the estimated ice surface temperature (IST) is less than 0.1 K in all seasons. Inclusion of channel 3 (3.7 μm) during the winter decreases the rms error by less than 0.003 K. The seasonal dependence of the coefficients is important, with errors in the range of 0.1 - 0.6 K when coefficients from one season are used with data from another. Similarly, mixing coefficients and data from different satellites results in average errors from 0.1 to 1.0 K. Overall, employing the IST coefficients results in increased accuracy of up to 0.6 K over SST coefficients developed for the North Atlantic and the Greenland Sea areas.

1. INTRODUCTION

Satellite data for the estimation of radiative and turbulent heat fluxes is becoming an increasingly important tool in large-scale studies of climate. One parameter needed in the estimation of these fluxes is surface temperature. Sea and land surface temperature (SST and LST) retrieval algorithms have been developed by using the thermal infrared window portion of the spectrum, with the degree of success dependent primarily upon the variability of the surface and atmospheric characteristics. The general approach to estimating surface temperature is to relate satellite observations to surface temperature observations with a regression model. Lacking sufficient observations, however, satellite radiances or brightness temperatures can be modeled by application of the radiative transfer equation. This approach is commonly used for SST retrieval [cf. *Minnett*, 1990; *Llewellyn-Jones et al.*, 1984; *Barton*, 1985]. A more complete review of SST algorithms is given by *McClain et al.* [1985]. For SST estimated using two "split-window" infrared channels (e.g., approximately 1 μm wide centered at 10.8 and 12.0 μm) an absolute accuracy of 0.5-1 K (rms error) has been obtained [*Llewellyn-Jones et al.*, 1984; *McClain et al.*, 1985]. Land surface temperature estimation is generally less accurate due to the larger variability of surface conditions, where errors of ±2-3 K are common [*Price*, 1983].

To our knowledge, little effort has been directed to the retrieval of the sea ice surface temperature (IST) in the Arctic, an area where the first effects of a changing climate are expected to be seen. The reason is not one of methodology, but rather our limited knowledge of atmospheric temperature, humidity, and aerosol profiles, the microphysical properties of polar clouds, and the spectral characteristics of the surface types found there. In this paper we present a means to correct for the atmospheric attenuation of satellite-measured clear sky brightness temperatures used in the retrieval of snow-covered ice surface temperature from the split-window thermal channels of the advanced very high resolution radiometer (AVHRR) sensors on board three of the NOAA series satellites. These corrections are specified for three different "seasons" and as a function of satellite viewing angle and are expected to be applicable to the perennial ice pack in the central Arctic Basin (Figure 1). We do not develop a completely new methodology; instead we modify a standard procedure for use with Arctic data. In this paper it is assumed that a valid cloud-clearing algorithm exists and that only clear sky radiances are being examined. The cloud clearing problem in polar satellite data is not trivial, however. For a review of polar cloud detection algorithms, see *Key and Barry* [1989] and *Sakellariou et al.* [1992].

Paper number 92JD00348.
0148-0227/92/92JD-00348$05.00

2. DATA

Analyses are based on atmospheric temperature and humidity profiles collected by rawinsonde from a Soviet ice island (NP-26), located at approximately 85°N 170°W during 1983-1987 (Figure 1). Generally, two observations per day were collected covering a vertical range of 0 - 25 km. Profiles that have at least 10 levels are retained in the analysis. Observations include temperature, dew point depression, wind speed, and wind direction. Ice crystal precipitation is not reported. For the years 1986-1987, surface-based cloud observations are also available. These observations include low, middle, and high cloud types, height of the cloud base, and cloud fraction.

Only clear sky profiles are used in this study (1986-1987), since the satellite thermal radiances under cloudy

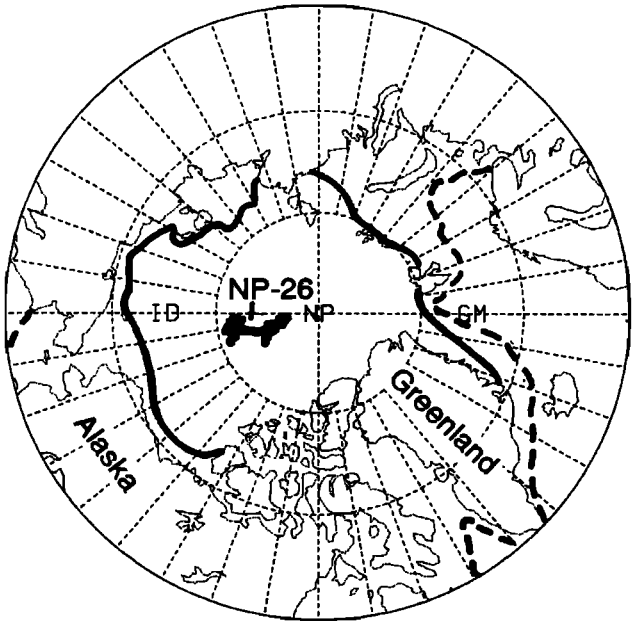

Fig. 1. Average minimum (solid) and maximum (dashed) sea ice extent in the Arctic Ocean. Also shown is the area covered by the NP-26 drifting ice island.

conditions will measure cloud top temperature and a significant amount of cloud cover will affect the lower tropospheric temperature structure. Clear sky is defined to be no more than 25% cloud cover by the surface observations. Clear sky "seasons" that differ in their vertical temperature and humidity structures are then defined. The seasons are determined objectively with a squared Euclidean distance clustering algorithm; the variables are temperature and humidity at each level. To reduce the degree of statistical dependence between levels, only one measurement per kilometer was used. The resulting seasons are winter (October through March), summer (June through August), and transition (April, May, and September). This analysis was also performed with three other methods: subjectively, clustering principal component scores, and using a simple correlation method. The only difference between them was in the placement of October. By temperature alone it is grouped with the transition months. When humidity profiles are also included in the analysis, however, it is more similar to the other winter months.

The resulting mean seasonal temperature profiles for clear, cloudy (greater than 75% cloud cover), and mixed conditions are shown in Figure 2. Differences reflect not only the near-surface temperatures but also the vertical temperature structure, which can also be seen in the monthly inversion frequencies reported by *Serreze et al.* [1991]. The effect of cloud on the surface radiation balance is evident in the clear and cloudy profiles where temperatures in the lower troposphere are higher under cloud cover in the winter and transition but lower under summer cloud cover. In addition, the summer surface inversion disappears under cloud cover. For comparison, the lowest 30 km of the standard subarctic summer and winter temperature profiles from the LOWTRAN 7 radiative transfer model data base [*Kneizys et al.*, 1988] are shown in Figure 3. The most obvious differences between the subarctic and Arctic profiles are the surface temperature and low-level inversion structure. In the Arctic profiles, standard deviation at all levels was computed for each parameter. The winter standard deviations of tropospheric clear sky temperature and dew point depression were computed for each layer, between 0 and 10 km. The maximum values occurred near the surface and were 6.8 K and 2.7 K, respectively. In

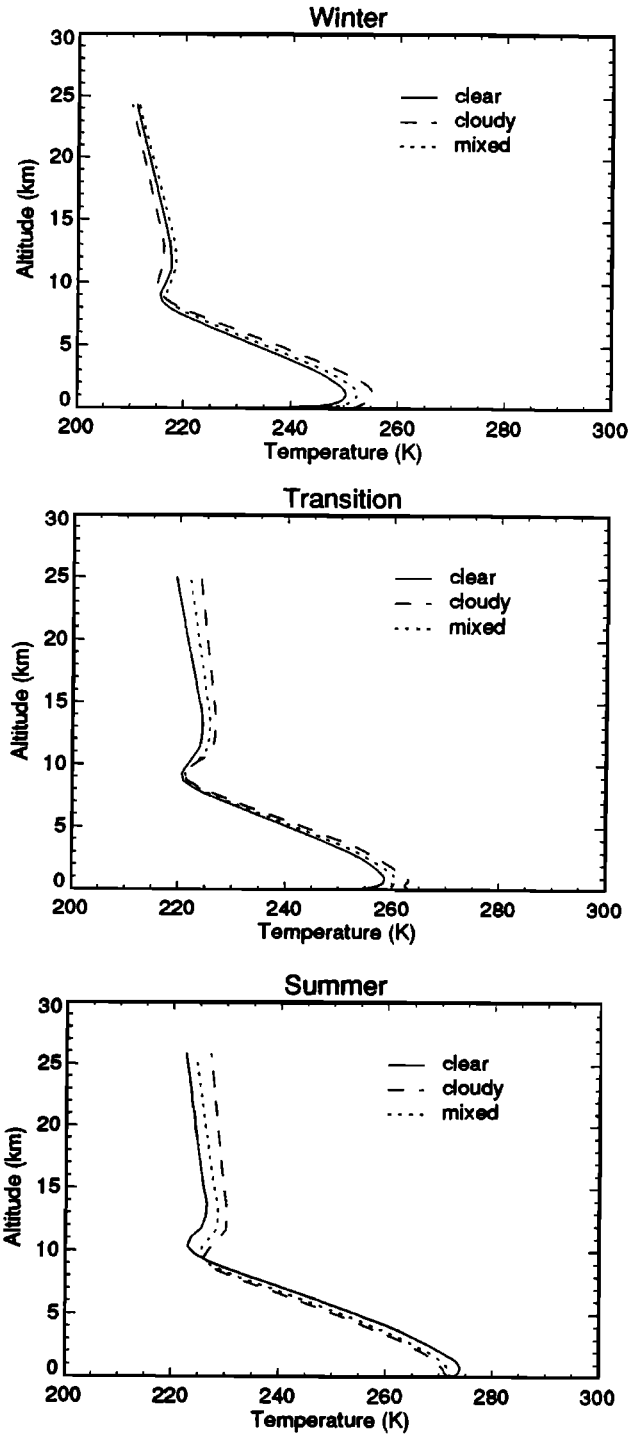

Fig. 2. Clear, cloudy, and mixed temperature profiles for the ice island data during winter (October - March), transition (April, May, September) and summer (June - August).

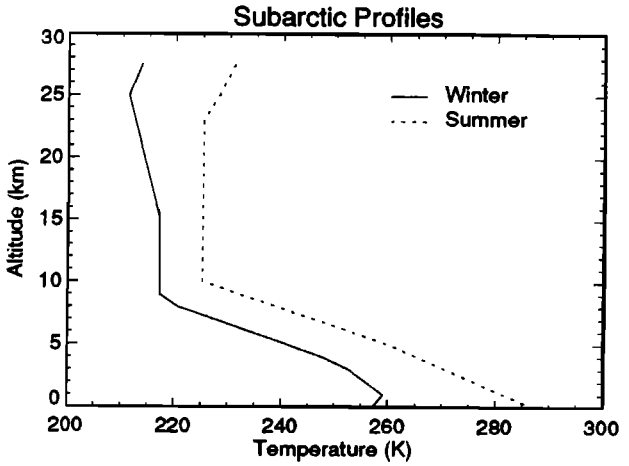

Fig. 3. Standard subarctic winter and summer temperature profiles.

summer the corresponding values are 4.5 K and 6.7 K, and in transition they are 7.9 K and 4.2 K. Interpretation of dew point depression variability requires care since the mean water vapor content is very low, generally less than 0.6 gm m^{-3}.

The AVHRRs on board the NOAA 7, 9, and 11 satellites are of interest in this study. Of the five AVHRR channels the three thermal channels (channel numbers 3, 4, and 5 centered at approximately 3.7, 11, and 12 μm) are simulated, and actual data are used for validation. NOAAs 8 and 10 are not used because they lack channel 5. First-order calibration was performed following the methods described by *NOAA* [1991] and *Lauritsen et al.* [1979]. Additional corrections were applied to the data to account for the nonlinear response of the thermal channels [*Weinreb et al.*, 1990]. Only NOAA 7 and 11 data were used in the validation. The AVHRR scan angle ranges from 0° to approximately 55°. Both local area coverage (LAC; 1.1-km field of view at nadir) and global area coverage (GAC; approximately 4 km) data are used in validation.

3. Retrieval Methodology

For the retrieval of SST a multichannel algorithm that corrects for atmospheric attenuation of upwelling radiation primarily due to water vapor absorption is commonly employed [e.g., *Barton et al.*, 1989]:

$$T_{ice} = a(\theta) + \sum_{i=3}^{5} b_i(\theta) T_i \qquad (1)$$

where $a(\theta)$ and $b_i(\theta)$ are satellite zenith angle-dependent coefficients and T_i are the satellite-measured brightness temperatures in the three AVHRR thermal channels. The coefficients are determined through a least squares regression procedure, where surface temperatures are regressed against modeled brightness temperatures. It is also possible to use differences between or ratios of two channels. Such an approach was taken by *Schluessel and Grassl* [1990] for SST retrieval at high latitudes.

Alternatives to computing a different set of coefficients for each scan angle increment, as shown in (1), were sought. Equations that include explicitly the scan angle have been presented [cf. *McClain et al.*, 1985]. Here we use the equation

$$T_{ice} = a + bT_4 + cT_5 + d[(T_4 - T_5)\sec\theta] \qquad (2)$$

for IST retrieval, where brightness temperatures are in Kelvin. The coefficients are given in the next section. The overall equation (2) produced the smallest standard error of all combinations of channels, channel differences, and scan angle functions tested, e.g., sec θ, [(1-sec θ)(T_4-T_5)], and similar variations. Although channel 3 could be included in (2), its use would be limited to winter analyses, since it measures reflected solar radiation as well as thermal emissions. The usefulness of this channel in IST retrieval is discussed in the next section.

To simulate radiances in the AVHRR thermal channels, the daily temperature and humidity profiles in each season are used with the LOWTRAN 7 (hereafter LOWTRAN) radiative transfer model [*Kneizys et al.*, 1988]. Earlier versions of LOWTRAN have been used in the retrieval of SST [e.g., *Barton et al.*, 1989]. LOWTRAN calculates atmospheric transmittance/radiance for wave numbers ranging from 0 to 50,000 cm^{-1} (0.2 μm to infinity) at a resolution of 20 cm^{-1} (for gaseous absorption) and includes calculations for multiple scattered radiation. The code may be initialized for standard or user-defined atmospheres, several cloud models, aerosol models, and specified solar and view geometry. Radiances are calculated at 5 cm^{-1} intervals (interpolated by LOWTRAN), equivalent to 0.06 μm at 11 μm. In this study, radiances are modeled for sensor scan angles from 0° to 60° in 10° increments. Atmospheric chemical composition and background tropospheric and stratospheric aerosols for the subarctic winter and summer models are used, since no such information is available from the ice islands. The optical properties of Arctic haze have not been extensively measured; model calculations [*Blanchet and List*, 1983] show that the volume extinction coefficient of Arctic haze is generally of the same order of magnitude as that of the tropospheric aerosols [*Tsay et al.*, 1989]. Therefore the use of tropospheric background aerosols is appropriate. The appropriate sensor response function (Figure 4) is applied to the calculated radiances, and radiances are then converted to brightness temperatures by inverting the Planck function at the central wavelength of the channel appropriate for the temperature range 230 - 270 K [*NOAA*, 1991]. The appendix provides additional detail on simulating satellite radiances.

The ice surface is assumed to be snow-covered year round. Directional surface emissivities for snow are modeled following the procedure of *Dozier and Warren* [1982]. Briefly, the single scattering albedo and asymmetry factor in the scattering phase function are calculated from the Mie equations, and the directional, wavelength-dependent emissivities are derived from the delta-Eddington approximation to the equation of radiative transfer. The directional emissivities are then integrated with the response function for channel i:

$$\varepsilon_i(\theta) = \frac{\int_{\lambda_1}^{\lambda_2} \varepsilon(\lambda,\theta)\phi_i(\lambda)\, d\lambda}{\int_{\lambda_1}^{\lambda_2} \phi_i(\lambda)\, d\lambda}$$

where $\varepsilon(\lambda,\theta)$ is the emissivity in direction θ at wavelength λ and φ is the sensor response function which is 0 outside of $[\lambda_1,\lambda_2]$. These emissivities are given in Table 1 for

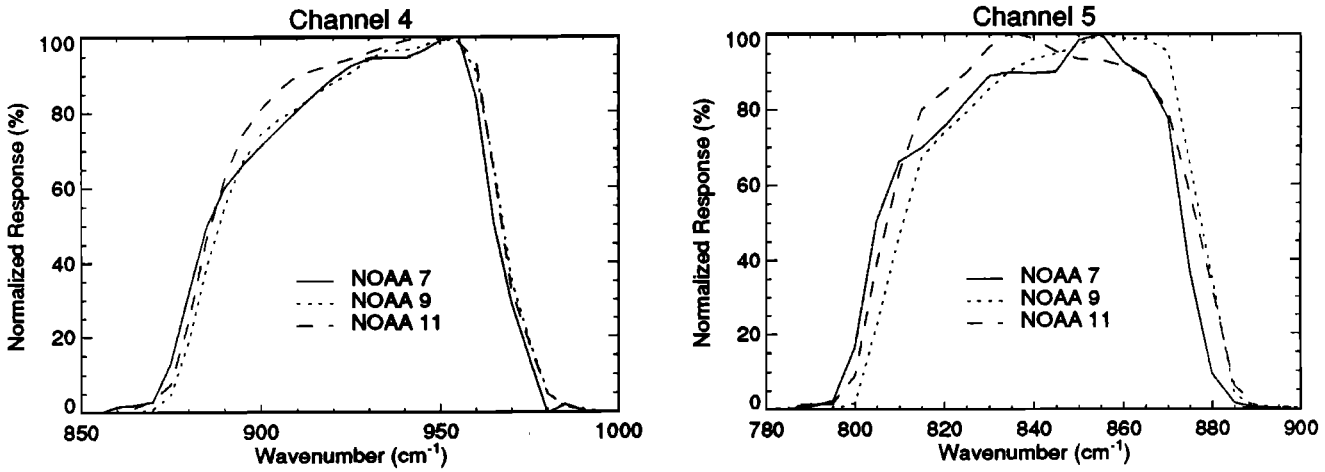

Fig. 4. Response functions for AVHRR channels 4 and 5 on NOAA 7, NOAA 9, and NOAA 11.

NOAA 7. The difference between the integrated emissivities for the three satellites examined here is approximately 0.0001, so we only use those modeled for NOAA 7. At the wavelengths of AVHRR channels 4 and 5 the emissivity is essentially insensitive to snow grain size as well as the amount of liquid water, up to 20% of the total particle volume. Additionally, these emissivities do not change significantly over the range of temperatures encountered and therefore are applicable to the snow types encountered year round. It is possible, however, that melt ponds will contaminate the field of view during the summer. We do not adjust emissivities to account for this phenomenon.

The use of the rawinsonde profiles in modeling the surface temperature requires an additional step, since the first measurement in each profile is the shelter temperature, not the surface temperature. (In the discussions that follow, the terms "skin" and "surface" temperature are used interchangeably.) The shelter-surface temperature difference can be significant: more than 10 K depending on the region and time of year [cf. *Stowe et al.*, 1988; *Rossow et al.*, 1989]. Therefore the (unknown) surface temperature for each profile is assigned a series of values representing the range of possible surface temperatures for the observed conditions during the month to which the profile belongs. An energy balance model is used to determine these surface temperatures, based on the observed range of shelter temperatures and wind speeds (the mean ±1 standard deviation) in the ice island data for each month. After *Maykut* [1982], the energy balance equation is

$$(1-\alpha)F_r - I_{ice} + F_L + \varepsilon\sigma T_{ice}^4 + F_s + F_e + F_c = 0$$

TABLE 1. Angular Emissivities of Snow in NOAA 7 AVHRR Channels 4 and 5

Scan Angle	Channel 4 Emissivity	Channel 5 Emissivity
0	0.9988	0.9961
10	0.9987	0.9958
20	0.9984	0.9949
30	0.9977	0.9933
40	0.9968	0.9908
50	0.9955	0.9872

where α is the albedo, ε is the longwave emissivity, σ is the Stefan-Boltzmann constant (in W m^{-2} K^{-4}), I_{ice} is the amount of shortwave energy that penetrates the ice and does not directly heat the surface, F_r and F_l are the downwelling shortwave and longwave radiation respectively, F_s and F_e are the sensible and latent heat fluxes, respectively, and F_c is the conductive heat flux. A flux toward the surface is positive. The sensible and latent heat fluxes are dependent in part upon the wind speed, air temperature, T_{ice}, and bulk transfer coefficients. Radiative fluxes are modeled based on the mean monthly temperature and humidity ice island profiles. Ice thicknesses are taken from *Maykut* [1982]. Three new profiles are created for each original clear sky profile, where the surface temperatures are the minimum, mean, and maximum equilibrium temperatures estimated by the model. This results in seasonal sample sizes of 750, 123, and 225 profiles for the winter, summer, and transition seasons, respectively.

4. Discussion

Coefficients for the estimation of IST are given in Tables 2-4 for NOAA 7, 9, and 11 satellites and are used with (2). Coefficients are given to five significant digits. (The rms error for using three significant digits rather than six in winter, for example, is 0.07 K, 0.003 K for four digits, and 0.0007 for five digits.) In all cases the coefficient of determination (R^2) is at least 0.98. Also shown is the root mean square (rms) error for the difference between the actual (energy balance model) surface temperature and the satellite-derived surface temperature. These errors are small—always less than 0.1 K and sometimes half that value—as a result of (1) the low water vapor content of the atmosphere and therefore little atmospheric attenuation, (2) the radiative transfer modeling approach, which does not incorporate satellite or ground-based instrument noise, and (3) natural variability in the polar atmosphere that was not captured in the ice island profiles. While the Arctic atmosphere is very dry, however, an atmospheric correction as in equation (2) is important. The uncorrected channel 4 and 5 brightness temperatures can be significantly different from the surface temperature; e.g., the mean T_{ice}-T_4 difference and its standard deviation (summer) are 0.66 and 0.43 K, 0.96

TABLE 2. Winter, Transition, and Summer Season Coefficients and rms Error Based on AVHRR Channels 4 and 5 for NOAA 7

Season	a	b	c	d	rms
Winter	-3.38568	6.28508	-5.27306	-2.45291	0.102
Transition	-3.77780	4.73209	-3.71850	-1.40115	0.074
Summer	-0.47429	3.77483	-2.77389	-0.56024	0.057

Season coefficients based on equation (2).

and 0.61 K for T_{ice}-T_5, -0.21 and 0.32 K for the winter channel 4 difference, and -0.23 and 0.43 K for channel 5 in winter, based on NOAA 7 simulated radiances at a surface emissivity of unity. Maximum differences are in the range of 1.7 to 2.3 K in summer and -2.5 to -3.5 in winter, for channels 4 and 5, respectively.

Due to a lack of Arctic surface and atmospheric data over the ice, it is difficult to define the area for which these coefficients apply. At present there is no evidence that temperature and humidity characteristics differ significantly over different portions of the perennial ice pack, but this cannot be confirmed. It has been found, however, that synoptic activity is quite different in the eastern Arctic (e.g., Kara Sea), affecting the strength and frequency of low-level inversions as well as humidity profiles [*Serreze et al.*, 1992]. We therefore consider these coefficients to apply to pack ice in the central Arctic Basin. The applicability of these coefficients to Antarctica is uncertain. The Arctic and Antarctic are both characterized by low temperatures, surface inversions, snow-covered surfaces, and low water vapor amounts. However, the temperatures and water vapor amounts are lower over Antarctica, although it is unknown how much lower the water vapor amounts are, by virtue of its higher elevation and lower incidence of cyclonic systems. Given this, one would expect there to be some difference between Antarctic surface temperatures estimated using the coefficients presented here and coefficients based on Antarctic temperature and humidity profiles, probably on the order of 0.1 - 0.3 K (see the discussion of SST coefficients below).

The utility of including channel 3 in surface temperature retrieval has been shown to be useful under certain conditions. For example, *Llewellyn-Jones et al.* [1984] found that triple-window simulations for the tropics were significantly better than split window, but not for temperate latitudes. *Barton* [1985] found channel 3 useful in both tropical and mid-latitude (Australia) locations. For IST retrieval, the use of channel 3 would be limited to winter analyses, since it has a reflected solar component as well as the thermal emissions. However, this channel is often noisy, especially during winter, when the amount of energy emitted at those wavelengths is small. To test its usefulness, winter is redefined as November - February, thereby avoiding a significant solar component in the upwelling radiance. Including channel 3 in (2) reduces the rms error by no more than 0.003 K or all satellites, which we do not consider a significant improvement in accuracy.

4.1. *Validation*

Validating the coefficients is difficult due to the lack of clear sky skin temperature measurements with corresponding satellite data. Therefore we use both measured and inferred surface temperatures. For example, AVHRR GAC data over the Barents Sea during July 1984 (NOAA 7) were used, with the surface temperature assumed to be near 273.15 K. This is a reasonable assumption for melting snow but may be an overestimate for ice due to its higher salinity. Over pack ice near the North Pole the mean estimated IST was 273.04 K. For a sample of pixels near the marginal ice zone with some melt ponds the mean IST was 273.27 K. Similarly, estimated ISTs in NOAA 11 AVHRR data over Greenland and Baffin Bay for July 1990 averaged 272.82 K over the ice sheet and 272.9 K over sea ice. The ice sheet location examined was the site of a Swiss Federal Institute of Technology (ETH) camp, which reported melt conditions (K. Steffen, personal communication, 1991).

GAC data during January 1984 north of Greenland were also used, where the estimated ISTs were compared to temperatures measured by drifting buoys [*Colony and Muñoz*, 1986]. There has been some discussion, although no formal study, concerning the accuracy of these buoy temperatures. During summer the buoy housing may experience radiational heating, and during winter they may be insulated by drifting snow. Comparison of estimated ISTs for 10 pixels around the location of two different buoys on January 7 yields mean temperature differences of 6 K for one buoy and 11 K for the other.

TABLE 3. Winter, Transition, and Summer Season Coefficients and rms Error Based on AVHRR Channels 4 and 5 for NOAA 9

Season	a	b	c	d	rms
Winter	-5.82059	7.81491	-6.79284	-3.34169	0.127
Transition	-6.06238	5.64562	-4.62267	-1.91927	0.089
Summer	0.49995	4.12165	-3.12356	-0.68087	0.067

Season coefficients based on equation (2).

TABLE 4. Winter, Transition, and Summer Season Coefficients and rms Error Based on AVHRR Channels 4 and 5 for NOAA 11

Season	a	b	c	d	rms
Winter	-5.39436	5.46800	-4.45233	-1.45853	0.071
Transition	-5.35487	4.47913	-3.46285	-0.97128	0.053
Summer	-1.76899	3.66554	-2.66249	-0.39676	0.053

Season coefficients based on equation (2).

The estimated ice surface temperatures were within 1 K of each other for each set of pixels. Differences of this magnitude were also reported by *Comiso* [1983, his Figure 3] for surface temperatures estimated from temperature humidity infrared radiometer (THIR) data, so that the use of the drifting buoys for validation does not appear to be useful.

Last, surface temperature measurements taken by a PRT 5 thermal radiometer during CEAREX in March 1989 are compared to NOAA 11 AVHRR data. The PRT 5 was flown on the NOAA P3 aircraft near Svalbard as part of the Arctic Gas and Aerosol Sampling Program (AGASP). The altitude of the instrument varied between 50 m and 4 km for the "clear" sky area of coincident aircraft/satellite data. While in concept this data should be useful for validation of the ISTs, it is problematic due to (1) time differences between the aircraft flight and the satellite overpass (a few hours), (2) an assumed unit emissivity in the calculation of PRT 5 temperatures, (3) geolocation errors for both the aircraft and the satellite data, and (4) the presence of aerosols and/or ice crystals above the aircraft. The last of these conditions greatly reduced the number of areas usable for validation. The geolocation problem dictates that the comparison between the PRT 5 and AVHRR data be done over a number of pixels rather than a single pixel. Given these problems, the best situation occurred when the aircraft was at an altitude of 160 m. The mean IST for a sample of four AVHRR pixels was 258.9 K, while the mean PRT 5 temperature (adjusted for an emissivity of 0.998) of four consecutive measurements 1 km apart was 259.04 K. Given the difficulties in comparing the two data sets, these results are encouraging.

4.2. *Dependencies and Atmospheric Considerations*

A potential problem in the retrieval of IST is the presence of ice crystal haze, or "diamond dust." It is particularly difficult to detect in AVHRR data because it is usually close to the surface and exhibits similar spectral properties. Values of the visible optical depth for ice crystal haze have been reported to range from 5 to 21 for wintertime and from 0.03 to 3 for springtime [*Curry et al.*, 1990]. The effect of varying optical depth of ice crystal haze on the estimated IST is illustrated indirectly in Figure 5, which shows brightness temperature differences between AVHRR channels 4 and 5 as a function of the optical depth of ice crystal haze over two ice surfaces: 5-cm-thick ice with a surface temperature of 256.62 K and 2 m ice with a surface temperature of 235.38 K. Mean January atmospheric conditions for the central Arctic are used at a satellite scan angle of 30°. The top of the ice crystal haze layer is near the top of the inversion, which has a temperature of 248 K. Using the coefficients developed here, estimated ISTs over the 2-m ice surface for the points indicated (in order of increasing optical depth) are 235.36, 237.51, 239.57, and 246.15 K. Depending on the cloud detection algorithm used, a temperature change of more than 2°-3° would probably signify cloud, so that in this example, diamond dust with optical depths greater than 0.34 do not present a problem in IST retrieval. At smaller optical depths, however, estimated ISTs could be in error. Given the uncertainty in the frequency of occurrence and spatial extent of this phenomenon, we do not attempt to adjust for it in the coefficients presented. Admittedly, this can be an important problem at certain times of the year.

The dependence of the coefficients on sensor scan angle has been found to be important by other investigators [cf. *Barton*, 1985; *Minnett*, 1990]. This is also the case for IST retrieval, although incorporating both channels 4 and 5 in (2) reduces the effect that increased path length at large scan angles has on the surface temperature estimation when scan angle is not taken into account explicitly. With the coefficients presented here the estimated surface temperature from (2) is very close to the surface tempera-

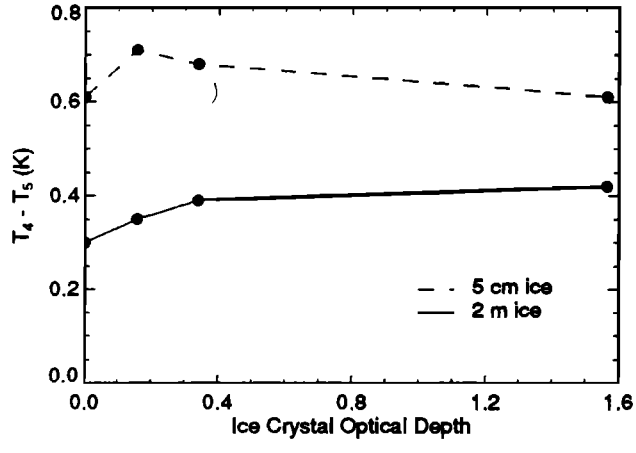

Fig. 5. Brightness temperature difference between AVHRR channels 4 and 5 as a function of the optical depth of ice crystal haze over two ice surfaces: 5-cm-thick ice with a surface temperature of 256.6 K and 2-m ice with a surface temperature of 235.4 K. Mean January atmospheric conditions for the central Arctic are used. The top of the ice crystal haze layer is near the top of the inversion, which has a temperature of 248.0 K. Satellite scan angle is 30°. Estimated ISTs over the 2-m ice surface for the points indicated (in order of increasing optical depth) are 235.36, 237.51, 239.57, and 246.15 K.

ture at all scan angles, while the estimated surface temperature using only channels 4 and 5 varies as a function of scan angle. Even though the differences are small, not including the scan angle explicitly results in an increased rms error of less than 0.1 K over using (2).

Coefficients in (2) were also computed assuming emissivities independent of wavelength and scan angle. In this case a different set of coefficients was produced at emissivities of 0.96 to 1.0 in increments of 0.01. Using the scan angle and wavelength dependent coefficients (Tables 2-4) with data based on fixed emissivity coefficients results in underestimates of 0.2 K for an emissivity of 1.0 and 0.6 K for an emissivity of 0.99 during summer with NOAA 7 simulated data. Since pure water has a slightly lower emissivity than pure snow (e.g., 0.992 at 11.9 μm and nadir), the estimated IST of an AVHRR pixel contaminated by summer meltponds would be incorrect by an amount somewhere between these two extremes depending on the proportion of water within the field of view.

The seasonal dependence of the coefficients is illustrated in Table 5, where coefficients from each season were applied to data from every other season. Results are shown for NOAA 9 and indicate errors between 0.1 K for transition coefficients with winter data and 0.6 K when summer coefficients are used with winter data. Similarly, the satellite dependence of the coefficients is shown in Table 6 for summer conditions. On the average, errors ranging from 0.1 to 1.0 K, depending on season, can be expected in applying coefficients derived for one satellite to data from another, the smallest errors occurring between NOAA 7 and 9 coefficients and data.

Using SST coefficients developed for the North Atlantic [*Llewellyn-Jones et al.*, 1984] and the Greenland Sea area [*Minnett*, 1990] to estimate IST would result in an underestimate of up to 0.7 K, largest in winter and at scan angles of 40° and greater. Not surprisingly, the difference is much larger (up to a 5.0 K overestimate) when tropical coefficients [*Llewellyn-Jones et al.*, 1984] are used. This comparison was made by using simulated radiances based on the directional emissivities, whereas the emissivity of the sea surface in the aforementioned studies was computed by using the Fresnel equations with the refractive index of water (actual values not given). These errors are similar to those reported by *Minnett* [1986], where SST was retrieved from North Atlantic data using coefficients from other regions.

Sensor characteristics and calibration also influence the retrieved IST. AVHRR GAC data are less noisy than LAC data and would result in a smoother IST field. Incorrect sensor calibration can produce large errors in estimated IST; errors in IST near Greenland of up to 3 K resulted from not including the nonlinear response correction in the calibration. Quantization of the signal (i.e., how much of a degree is represented by one digital count) introduces additional error. Some of these factors affect whether or not there is a systematic difference between the estimated ISTs and the true (measured) IST—the system bias—but due to the small quantity of coincident surface/satellite measurements, the degree of influence is impossible to assess. Therefore no empirical corrections to the forward model are suggested, which would otherwise account for sensor and other factors such as radiosonde accuracy and the treatment of the stratosphere above the known profile.

TABLE 5. The rms Error in Applying Coefficients (NOAA 9) Developed for One Season to Data From Another

	Data from		
Coefficients	Winter	Summer	Transition
Winter	0	0.403	0.128
Summer	0.587	0	0.342
Transition	0.117	0.219	0

TABLE 6. The rms Error in Applying Coefficients (Summer) Developed for One Satellite to Data From Another

	Data from		
Coefficients	NOAA 7	NOAA 9	NOAA 11
NOAA 7	0	0.272	0.655
NOAA 9	0.296	0	1.017
NOAA 11	0.682	0.961	0

5. SUMMARY AND CONCLUSIONS

The relationship between AVHRR clear sky thermal radiances and the surface (skin) temperature of central Arctic snow-covered sea ice is examined through forward calculations of the radiative transfer equation. Temperature and humidity profiles and cloud data from ice islands during 1986-1987 are used. Coefficients that correct for atmospheric attenuation are given for three Arctic clear sky "seasons," as defined through statistical analysis of the daily profiles, for the NOAA 7, 9, and 11 satellites. Modeled directional emissivities, different in the two split-window channels, are used. While the sensor scan angle is included explicitly in the correction equation, its effect in the dry Arctic atmosphere is small, generally less than 0.1 K. The coefficients presented are for use with AVHRR channels 4 and 5 (11 and 12 μm) and the sensor scan angle. With this method the rms error in the estimated ice surface temperature is less than 0.1 K in all seasons. Inclusion of channel 3 (3.7 μm) during the winter decreases the rms error by less than 0.003 K.

The seasonal dependence of the coefficients is important, with rms errors in the range of 0.1 - 0.6 K when coefficients are applied across seasons. Similarly, using coefficients from one satellite with data from another results in average errors from 0.1 to 1.0 K. Overall, employing the IST coefficients results in increased accuracy of up to 0.6 K over SST coefficients developed for the North Atlantic and the Greenland Sea areas. While this difference is small in terms of outgoing longwave radiation, it is important for long-term climate monitoring. Modeled ice crystal haze during January indicates that at small optical depths the haze may not be detected as cloud and could result in IST errors of up to 2°.

Two important problems remain in the retrieval of ice

surface temperature. First, until a reliable method of cloud clearing becomes accepted by the science community, IST retrieval results will have an additional level of uncertainty. Second, coincident satellite, surface, and atmosphere measurements over sea ice must be taken across the Arctic and in all seasons before the bias of these IST coefficients can be accurately determined.

APPENDIX

Assuming that clouds do not contaminate the satellite scene, that the remaining atmosphere is nonscattering, and that the surface is nonblack, then the radiative transfer equation for the upward monochromatic radiance $L(\lambda,\theta)$ at wavelength λ and satellite view angle θ can be expressed as

$$L(\lambda,\theta) = \varepsilon_\lambda(\theta)B_\lambda(T_s)e^{-\sigma_\lambda} + \int_0^{\sigma_\lambda} B_\lambda[T(\sigma'_\lambda)]e^{-\sigma'_\lambda}d\sigma'_\lambda + [(1-\varepsilon_\lambda(\theta)]e^{-\sigma_\lambda}\int_{\sigma'_\lambda}^{0} B_\lambda[T(\sigma'_\lambda)]e^{-\sigma'_\lambda}d\sigma'_\lambda$$

where ε_λ is the emissivity of the surface (which is assumed equal at all λ within a channel in this study), T_s is the surface temperature in Kelvin, σ_λ is the optical depth of the slant path, and $B_\lambda(T)$ is the Planck function at temperature T. The first term on the right is the contribution from the surface, the second is from atmospheric emission, and the third represents downward atmospheric emission that has been reflected upward. The surface contribution is assumed to be the dominant one for the IST retrieval outlined in (2), which can be illustrated by estimating radiances in the two split-window channels using the clear sky Arctic mean and subarctic standard winter and summer profiles with identical surface temperatures. The maximum difference in radiances is 0.05 W m^{-2} sr^{-1}, indicating that the vertical temperature distribution of the relatively dry Arctic atmosphere plays a relatively small role in the attenuation of upwelling longwave radiation.

To simulate the satellite radiance, the radiances at wavelengths across each channel must be integrated with the sensor response function:

$$L_i = \frac{\int_{\lambda_1}^{\lambda_2} L(\lambda,\theta)\phi_i(\lambda)\,d\lambda}{\int_{\lambda_1}^{\lambda_2} \phi_i(\lambda)\,d\lambda}$$

where L_i is the channel i radiance, $\Phi_i(\lambda)$ is the channel's response function, and λ_1 and λ_2 are the lower and upper limits of the channel, i.e., where the response is 0. Using a rectangular response function defined by the half-amplitude full-width portion of the actual channel response (but with 100% response at all wavelengths) instead of the full response function results in brightness temperature differences of the order of 0.05 K in channel 4 and 0.5 K in channel 5 (January conditions). These figures are valid for two central wavelengths used in the conversion of radiance to brightness temperature: that from the full response function or one based on Planck radiances specifically for the half-amplitude function.

Acknowledgments. J. Key was supported under NASA grant NAGW-2407 (University of Washington subcontract 721566) and ONR grant N00014-90-J-1840. M. Haefliger was supported under NASA grant NAGW-2158. Thanks are due to M. Serreze and J. Kahl for providing the ice island atmospheric data (NA85RAH05066), R. Schnell for the aircraft PRT-5 CEAREX data, K. Steffen for a sample of the Greenland ETH data (which is part of an ongoing project with results to be reported subsequently), and R. Lindsay and the anonymous reviewers for a thorough review of an earlier version of the manuscript.

REFERENCES

Barton, I. J., Transmission model and ground-truth investigation of satellite-derived sea surface temperatures, *J. Clim. Appl. Meteorol.*, *24*, 508-516, 1985.

Barton, I. J., A. M. Zavody, D. M O'Brien, D. R. Cutten, R. W. Saunders, and D. T. Llewellyn-Jones, Theoretical algorithms for satellite-derived sea surface temperatures, *J. Geophys. Res.*, *94*(D3), 3365-3375, 1989.

Blanchet, J., and R. List, Estimation of optical properties of arctic haze using a numerical model, *Atmos. Ocean*, *21*, 444-465, 1983.

Colony, R., and E.A. Muñoz, Arctic Ocean buoy program data report: 1 January 1984 - 31 December 1985, 277 pp., Polar Sci. Center, Appl. Phys. Lab., Univ. Wash., Seattle, Oct. 1986.

Comiso, J. C., Sea ice effective microwave emissivities from satellite passive microwave and infrared observations, *J. Geophys. Res.*, *88*(C12), 7686-7704, 1983.

Curry, J. A., F. G. Meyer, L. F. Radke, C. A. Brock, and E. E. Ebert, Occurrence and characteristics of lower tropospheric ice crystal in the Arctic, *Int. J. Climatol.*, *10*, 749-764, 1990.

Dozier, J., and S. G. Warren, Effect of viewing angle on the infrared brightness temperature of snow, *Water Resour. Res.*, *18*(5), 1424-1434, 1982.

Key, J., and R. G. Barry, Cloud cover analysis with arctic AVHRR data, 1, Cloud detection, *J. Geophys. Res.*, *94*(D15), 18,521-18,535, 1989.

Kneizys, F. X., E. P. Shettle, L. W. Abreu, J. H. Chetwynd, G. P. Anderson, W. O. Gallery, J. E. A. Selby, and S. A. Clough, Users guide to LOWTRAN 7, *Rep. AFGL- TR-88-0177*, 137 pp, Environmental Research Papers, No. 1010, Air Force Geophys. Lab., Bedford, Mass., 1988.

Lauritson, L., G. G. Nelson, and R. W. Port, Data extraction and calibration of TIROS-N/NOAA A-G radiometer, *NOAA Tech. Memo., NESS 107*, 81 pp., Natl. Oceanic and Atmos. Admin., Boulder,Colo., 1979.

Llewellyn-Jones, D. T., P. J. Minnett, R. W. Saunders, and A. M. Zavody, Satellite multichannel infrared measurements of sea surface temperature of the northeast Atlantic Ocean using AVHRR/2, *Q. J. R. Meteorol. Soc.*, *110*, 613-631, 1984.

Maykut, G. A., Large-scale heat exchange and ice production in the central Arctic, *J. Geophys. Res.*, *87*(C10), 7971-7984, 1982.

McClain, E. P., W. G. Pichel, and C. C. Walton, Comparative performance of AVHRR-based multichannel sea surface temperatures, *J. Geophys. Res.*, *90*, 11,587-11,601, 1985.

Minnett, P. J., A numerical study of the effects of anomalous North Atlantic atmospheric conditions on the infrared measurement of sea surface temperature from space, *J. Geophys. Res.*, *91*(C7), 8509-8521, 1986.

Minnett, P. J., The regional optimization of infrared measurements of sea surface temperature from space, *J. Geophys. Res.*, *95*(C8), 13,497-13,510, 1990.

NOAA, NOAA Polar Orbiter Data User's Guide, U.S. Dept. of Commer., Nat. Ocean. and Atmos. Admin., NESDIS, Boulder, Colo., Feb. 1991.

Price, J. C., Estimating surface temperatures from satellite thermal infrared data—A simple formulation for the atmospheric effect, *Remote Sens. Environ.*, *13*, 353-361, 1983.

Rossow, W. B., L. C. Garder, and A. A. Lacis, Global, seasonal cloud variations from satellite radiance measurements, I, Sensitivity of analysis, *J. Climate*, *2*, 419-458, 1989.

Sakellariou, N. K., H. G. Leighton, and Z. Li, Identification of clear and cloudy pixels at high latitudes from AVHRR radiances, *Int. J. Remote Sen.*, in press, 1992.

Schluessel, P., and H. Grassl, SST in polynias: A case study, *Int. J. Remote Sens.*, *11*(6), 933-945, 1990.

Serreze, M. C., J. D. Kahl, and R. C. Schnell, Low-level temperature inversions of the Eurasian Arctic and comparisons with Soviet drifting station data, *J. Climate*, in press, 1992.

Stowe, L. L., C. G. Wellemeyer, T. F. Eck, H. Y. M. Yeh, and The Nimbus-7 Cloud Data Processing Team, Nimbus-7 global cloud climatology, I, Algorithms and validation, *J. Climate*, *1*, 445-470, 1988.

Tsay, S.-C., K. Stamnes, and K. Jayaweera, Radiative energy budget in the cloudy and hazy arctic, *J. Atmos. Sci.*, *46*(7), 1002-1018, 1989.

Weinreb, M. P., G. Hamilton, and S. Brown, Nonlinearity corrections in calibration of advanced very high resolution radiometer infrared channels, *J. Geophys. Res.*, *95*(C5), 7381-7388, 1990.

J. Key and M. Haefliger, Cooperative Institute for Research in Environmental Sciences, Division of Cryosphric and Polar Processes, University of Colorado, Boulder, Colorado 80309-0449.

(Received October 31, 1991;
revised January 13, 1992;
accepted January 15, 1992.)